

1 **Pervasive Remagnetization of Detrital Zircon Host Rocks in the Jack Hills, Western**  
2 **Australia and Implications for Records of the Early Geodynamo**

3  
4 Benjamin P. Weiss<sup>a,b\*</sup>, Adam C. Maloof<sup>c</sup>, Nicholas Tailby<sup>d,e</sup>, Jahandar Ramezani<sup>a</sup>, Roger  
5 R. Fu<sup>a</sup>, Veronica Hanus<sup>a</sup>, Dustin Trail<sup>f</sup>, E. Bruce Watson<sup>d,e</sup>, T. Mark Harrison<sup>g</sup>, Samuel  
6 A. Bowring<sup>a</sup>, Joseph L. Kirschvink<sup>h,i</sup>, Nicholas L. Swanson-Hysell<sup>b</sup>, Robert S. Coe<sup>j</sup>

7  
8 <sup>a</sup>Department of Earth, Atmospheric, and Planetary Sciences, Massachusetts Institute of  
9 Technology, 77 Massachusetts Avenue, Cambridge, MA 02139, USA

10 <sup>b</sup>Department of Earth and Planetary Science, University of California (UC), Berkeley,  
11 Berkeley CA, 94720, USA

12 <sup>c</sup>Department of Geosciences, Princeton University, Guyot Hall, Washington Road,  
13 Princeton, NJ 08544, USA

14 <sup>d</sup>Department of Earth and Environmental Sciences, Rensselaer Polytechnic Institute,  
15 Troy, New York 12180, USA.

16 <sup>e</sup>New York Center for Astrobiology, Rensselaer Polytechnic Institute, Troy, New York  
17 12180, USA.

18 <sup>f</sup>Department of Earth and Environmental Sciences, Box 270221, University of Rochester  
19 Rochester, NY 14627

20 <sup>g</sup>Institute of Geophysics and Planetary Physics, UC, Los Angeles, Los Angeles, CA  
21 90095, USA

22 <sup>h</sup>Division of Geological and Planetary Sciences, California Institute of Technology, USA

23 <sup>i</sup>Earth-Life Science Institute, Tokyo Institute of Technology, Meguro, Tokyo, Japan.

24 <sup>j</sup>Department of Earth and Planetary Sciences, UC, Santa Cruz, CA 95064, USA

25 \*To whom correspondence should be addressed: bpweiss@mit.edu

26  
27 Corresponding author. Tel.: +1-617-324-0224, fax: +1-617-258-7401.

28 Email address: bpweiss@mit.edu (B. P. Weiss)

29  
30 Submitted to *Earth and Planetary Science Letters*

31

32 It currently is unknown when Earth's dynamo magnetic field originated.  
33 Paleomagnetic studies indicate that a field with an intensity similar to that of the  
34 present day existed 3.5 billion years ago (Ga). Detrital zircon crystals found in the  
35 Jack Hills of Western Australia are some of the very few samples known to  
36 substantially predate this time. With crystallization ages ranging from 3.0-4.38 Ga,  
37 these zircons might preserve a record of the missing first billion years of Earth's  
38 magnetic field history. However, a key unknown is the age and origin of  
39 magnetization in the Jack Hills zircons. The identification of >3.9 Ga (i.e., Hadean)  
40 field records requires first establishing that the zircons have avoided  
41 remagnetization since being deposited in quartz-rich conglomerates at 2.65-3.05 Ga.  
42 To address this issue, we have conducted paleomagnetic conglomerate, baked  
43 contact, and fold tests in combination with U-Pb geochronology to establish the  
44 timing of the metamorphic and alteration events and the peak temperatures  
45 experienced by the zircon host rocks. These tests include the first conglomerate test  
46 directly on the Hadean-zircon bearing conglomerate at Erawandoo Hill. Although  
47 we observed little evidence for remagnetization by recent lightning strikes, we found  
48 that the Hadean zircon-bearing rocks and surrounding region have been  
49 pervasively remagnetized, with the final major overprinting likely due to thermal  
50 and/or aqueous effects from the emplacement of the Warakurna large igneous  
51 province at ~1070 million years ago (Ma). Although localized regions of the Jack  
52 Hills might have escaped complete remagnetization, there currently is no robust  
53 evidence for pre-depositional (>3.0 Ga) magnetization in the Jack Hills detrital  
54 zircons.

55

56

57

58

59

60

61

62

63

64

65

66 **Keywords:** geodynamo; paleointensity; core; Jack Hills; detrital zircons; Hadean earth

67

## 68 **1. The early geodynamo and the Jack Hills**

69 The oldest known unmetamorphosed rocks indicate the existence of an active  
70 dynamo magnetic field with intensity 50-70% of the present day at 3.450 Ga (Biggin et  
71 al., 2011; Tarduno et al., 2010). Due to the lack of older low metamorphic grade rocks,  
72 the existence and intensity of the geodynamo during the first ~1 billion years of Earth  
73 history—the Hadean eon (>4.0 Ga) and subsequent Eoarchean era (3.6-4.0 Ga)—remain  
74 unknown. The early history of the field has important implications for planetary thermal  
75 evolution, the physics of dynamo generation, and the oxidation state of the atmosphere  
76 (Gomi et al., 2013; Gubbins et al., 2004; Lammer et al., 2008; Nimmo et al., 2004;  
77 Tarduno et al., 2014; Ziegler and Stegman, 2013).

78 The only materials of which we are aware that could possibly retain  
79 paleomagnetic records substantially predating 3.5 Ga are detrital zircon crystals found in  
80 upper greenschist facies (i.e., ~350-450°C peak metamorphic temperature)  
81 metaconglomerates from Erawandoo Hill in the Jack Hills of Western Australia (Holden  
82 et al., 2009). With U-Pb crystallization ages ranging from 3.05-4.38 Ga, these zircons  
83 are the oldest known Earthly materials. Ferromagnetic inclusions in these zircons have  
84 the potential to yield the oldest known records of the geomagnetic field.

85 The pebble metaconglomerates containing >4 Ga old zircons were deposited at  
86 2.65-3.05 Ga (Rasmussen et al., 2010) and have been subsequently metamorphosed and  
87 heavily weathered (Spaggiari, 2007b). A key difficulty with establishing the age of the  
88 zircons' magnetization is that these post-depositional processes could have completely  
89 remagnetized their inclusions without disturbing the zircons' U-Pb systematics (Mezger  
90 and Krogstad, 1997). Laboratory diffusion experiments indicate that a 1 billion year-  
91 thermal event at ~750°C, which exceeds the Curie points of common ferromagnetic  
92 minerals ( $\leq 675^\circ\text{C}$ ), will produce just 1% Pb loss from a 100  $\mu\text{m}$  radius non-metamict  
93 zircon (Cherniak and Watson, 2000). Therefore, a zircon's magnetization could be far

94 younger than its crystallization age or even disturbance ages inferred from U-Pb  
95 discordance. Furthermore, even if could be established that the zircons have not been  
96 thermally remagnetized, they still might not retain an ancient magnetization if their  
97 ferromagnetic inclusions are secondary (Rasmussen et al., 2011).

98 A first step toward constraining the age of magnetization in the zircon grains is to  
99 establish whether their host conglomerates have been remagnetized since their deposition  
100 at 2.65-3.05 Ga. If the rocks have been thermally remagnetized to temperatures  
101 exceeding the Curie point of ferromagnetic inclusions in the zircons, this would require  
102 that the inclusions themselves were also completely remagnetized by the same event.  
103 Alternatively, if the host rocks have been primarily aqueously rather than thermally  
104 remagnetized, ancient magnetization might still be retained within primary ferromagnetic  
105 inclusions armored against penetrative fluid flow by the surrounding host zircon.  
106 Nevertheless, even this favorable case would still leave unknown whether the zircons  
107 were remagnetized following crystallization but before deposition.

108 The most direct methods for establishing whether rocks retain ancient  
109 magnetization are paleomagnetic field tests (Graham, 1949). The basis of the fold test  
110 (McElhinny, 1964) is that magnetization that predates (postdates) folding will be less  
111 (more) directionally scattered in bedding-corrected coordinates. Similarly, in the baked  
112 contact test (Buchan, 2007), country rocks located outside the remagnetization aureole of  
113 a younger igneous intrusion and that have magnetization predating (postdating) the  
114 intrusion will be magnetized in a different direction from (similar direction to) that of the  
115 intrusion. In the conglomerate test, magnetization in clasts of a conglomerate that  
116 predates (postdates) deposition of the conglomerates will be collectively randomly  
117 (nonrandomly) oriented (Watson, 1956). A robust conglomerate test will also  
118 demonstrate that the magnetization within individual clasts is consistently oriented in  
119 order to exclude the possibility that random cobble magnetization directions resulted  
120 from fine-scale heterogeneous remagnetization of the conglomerate after deposition.

121 Recently, Tarduno and Cottrell (2013) reported a paleomagnetic conglomerate  
122 test on a quartz-cobble metaconglomerate from the Jack Hills. They identified a high-  
123 temperature magnetization component in 27 cobbles that thermally demagnetized from  
124 ~540°C and 580°C and was randomly oriented to >95% confidence. They proposed that

125 this positive conglomerate test indicates that the host rocks had not been thermally  
126 remagnetized to  $>540^{\circ}\text{C}$  since their deposition. However, this conglomerate test has  
127 several limitations, the most important of which are:

128 (i) The test was conducted 0.6 km from Erawandoo Hill, with the intervening  
129 stratigraphy obscured by cover and containing bedding-parallel faults and  
130 shear zones (Spaggiari, 2007b). Therefore, the thermal history of the cobbles  
131 might differ greatly from that of the  $>4.0$  Ga zircon-bearing Erawandoo Hill  
132 conglomerate.

133 (ii) The abundance of zircons with  $\sim 1700$  Ma ages [with one grain as young as  
134 1220 Ma (Grange et al., 2010)] in similar, nearby cobbles means that the  
135 conglomerate test may only constrain remagnetization events following as  
136 much as 1400 million years after the deposition of the Erawandoo Hill  
137 Hadean-zircon bearing conglomerate and after many of the major  
138 metamorphic events known to have affected the region.

139 (iii) For most samples, no overprinting magnetization was identified with a  
140 direction unambiguously corresponding to known metamorphic events as  
141 indicated by Australia's polar wander path. Such overprint are expected if  
142 the cobbles are as old as the 2.65-3.0 Ga Erawandoo Hill conglomerate.

143 We conducted two trips to the Jack Hills in 2001 and 2012 to acquire samples for  
144 paleomagnetic conglomerate, baked contact, and fold tests and geochronometry that  
145 address these limitations. Our goal was to establish the intensity and timing of  
146 metamorphic and alteration events to constrain the remagnetization processes  
147 experienced by the zircons' host rocks directly at Erawandoo Hill and the surrounding  
148 region. Here we report the results of paleomagnetic and radioisotopic analyses of these  
149 samples and their implications for the preservation of ancient paleomagnetic records in  
150 the Jack Hills zircons.

151

## 152 **2. Geology of the Jack Hills**

153 The host rocks of the ancient detrital zircons in the Jack Hills are part of an  
154 apparently  $\sim 2$  km thick sedimentary succession in fault contact with the surrounding  
155 granites and granitic gneisses of the Archean Narryer Terrane (Maas et al., 1992;

156 Spaggiari, 2007a; Wilde, 2010) (Fig. 1). The supracrustal rocks are steeply dipping,  
157 recumbently folded and thought to pinch out at depth in contact with underlying granite.  
158 There are four main sedimentary associations: (1) Archean chert and banded iron  
159 formation along the northern and southern margins of the belt, (2) Archean pelitic schists,  
160 (3) mature Archean clastic sandstones, quartzites, and conglomerates that include the  
161 2.65-3.05 Ga Hadean detrital zircon host rocks, and (4) Proterozoic quartz-rich rocks  
162 (Eriksson and Wilde, 2010; Spaggiari et al., 2007; Wilde and Pidgeon, 1990). The  
163 contacts between and within these four associations are often shear zones and/or are  
164 obscured by cover. The Hadean detrital zircons have been found almost exclusively  
165 within ~1 km of Erawandoo Hill, mainly in a metaconglomerate containing  
166 metamorphically elongated and flattened, cm-sized quartzitic pebbles set in a sandy  
167 matrix (Spaggiari, 2007b)

168 Because the 2.65-3.05 Ga depositional age of the Hadean zircon-bearing  
169 sediments postdates the surrounding ~3.10-3.73 Ga gneisses and porphyritic granitoid  
170 rocks (Pidgeon and Wilde, 1998; Spaggiari et al., 2008), the detrital zircon host rocks  
171 largely avoided high-grade metamorphism associated with these intrusions. The zircon  
172 host rocks nevertheless experienced multiple episodes of thermal metamorphism and  
173 aqueous alteration. In particular, quartz–biotite–chloritoid assemblages in siliciclastic  
174 rocks indicate upper greenschist facies metamorphism, while grunerite in surrounding  
175 banded iron formation and calcic plagioclase-hornblende assemblages in mafic schists  
176 indicate at least localized amphibolite facies metamorphism (Spaggiari, 2007b; Wilde  
177 and Pidgeon, 1990). Monazite-xenotime and Ti-in-quartz thermometry suggest that the  
178 Erawandoo Hill conglomerates reached ~346-487°C (Rasmussen et al., 2010). As  
179 described in the Supplemental Materials (SM), there were at least four major thermal and  
180 deformational events that likely affected the zircon host rocks: (i) thermal metamorphism  
181 at 2654 Ma due to monzogranite intrusions linked to the assembly of the Yilgarn craton;  
182 (ii) thermal disturbances associated with the 1960-2005 Ma Glenburgh orogeny; (iii)  
183 thermal disturbances and large-scale shearing associated with the Capricorn orogeny at  
184 1780-1830 Ma; and (iv) emplacement of the Marnda Moorn and Warakurna large  
185 igneous provinces (LIPs) at ~1210 and ~1070 Ma, respectively.

186 We conducted three baked contact tests associated with a dolerite dyke intruding  
187 quartzitic rocks and pebble conglomerate, two fold tests associated with folds within  
188 quartzitic rocks, three conglomerate tests associated with the Erawandoo Hill Hadean  
189 zircon-bearing pebble conglomerates, and three conglomerate tests associated with  
190 cobble conglomerates of similar lithology and in close proximity to those studied by  
191 Tarduno and Cottrell (2013). We also sampled lithologies distributed throughout the  
192 central Jack Hills, including a 2654 Ma monzogranite intruding the supracrustal rocks, to  
193 establish the larger spatial scale of remagnetization from both the dolerite and the  
194 monzogranite intrusions. Our sample localities are shown in Fig. 1.

195

### 196 **3. Rock magnetism and petrography**

197 *3.1. Overview.* We characterized the ferromagnetic mineralogy and magnetic properties  
198 of the Jack Hills rocks to establish their fidelity for recording remagnetization events and  
199 to constrain their alteration history. We conducted rock magnetic analyses of chips and  
200 powders and optical and electron microscopy of polished 30  $\mu\text{m}$  thin sections from  
201 samples of the major lithologies subjected to paleomagnetic analyses.

202

203 *3.2. Thermal demagnetization of three-axis isothermal remanent magnetization (IRM).*  
204 To determine peak unblocking temperature as a function of coercivity, twenty samples  
205 were each given a three-component IRM and progressively thermally demagnetized. The  
206 composite IRM was produced by exposure to 4 T along the sample  $z$ -axis followed by  
207 0.36 T and then 0.12 T along the  $x$ - and  $y$ -axes, respectively. Given the peak coercivities  
208 for common ferromagnetic minerals (Dunlop and Özdemir, 1997),  $z$ -axis magnetization  
209 should be carried by hematite (Néel temperature  $\sim 675^\circ\text{C}$ ), goethite (Néel temperature of  
210  $\sim 50$ - $120^\circ\text{C}$ ), and pyrrhotite (Néel temperature  $\sim 320^\circ\text{C}$ ),  $x$ -axis magnetization should  
211 dominantly reflect pyrrhotite and magnetite, and  $y$ -axis magnetization should reflect  
212 pyrrhotite, magnetite and titanomagnetite (Dekkers, 1989; Lowrie, 1990; Özdemir and  
213 Dunlop, 1996). Moment measurements were acquired with a 2G Enterprises  
214 Superconducting Rock Magnetometer (SRM) 755 in the UC Berkeley Paleomagnetism  
215 Laboratory (Kirschvink et al., 2008).

216 The results (Figs. 2 and S2) show that the monzogranite contains predominantly  
217 magnetite and goethite with a small amount of hematite, while the dolerite contains  
218 mostly magnetite with a small quantity of pyrrhotite and hematite. Quartzitic rocks from  
219 the fold test sites contain hematite and goethite (at site D197) and pyrrhotite, goethite,  
220 and lesser magnetite (at site D102). Erawandoo Hill conglomerate pebble clasts contain  
221 almost exclusively pyrrhotite, the Erawandoo matrix contains additional hematite, and  
222 cobble clasts from the cobble conglomerate contain dominantly pyrrhotite with lesser  
223 hematite and minor quantities of magnetite.

224

### 225 *3.3. Other rock magnetic experiments.*

226 We measured temperature-dependent susceptibility of cobbles from ~25-700°C in  
227 in both air and Ar (Fig. 3). When heating in air, most cobbles heated in air showed weak  
228 susceptibility signals (Fig. 3C, F and S1B), with a single exception that exhibited a  
229 susceptibility peak indicating the generation magnetite (Fig. 3A), possibly from sulfide  
230 alteration. Heating in Ar above ~400°C led to the generation magnetite (Fig. 3B, D, E,  
231 G) presumably due to reduction of hematite or other oxidized phases. There is no  
232 evidence for pyrrhotite in any of our susceptibility data.

233 We also conducted low temperature cycling experiments on both fresh cobble  
234 samples as well as those previously subjected to the high temperature susceptibility  
235 measurements. Low temperature transitions (Fig. 3E and SM) indicate the presence of  
236 pyrrhotite along with some magnetite. These data also confirm that magnetite was  
237 produced during the susceptibility measurements in Ar (see Fig. 3E and F and SM).

238 Our room temperature hysteresis and back field remanence measurements (Fig.  
239 S3 and SM) show that the mean ferromagnetic grain size for all analyzed samples is  
240 pseudo single domain, with the monzogranites likely containing a mixture of  
241 multidomain and single domain magnetite and hematite plus goethite, respectively.

242

243 *3.4. Optical and electron microscopy.* We conducted optical microscopy, backscattered  
244 electron microscopy (BSEM), electron dispersive spectroscopy, and wavelength  
245 dispersive spectroscopy (WDS) to constrain the composition, grain size, textural  
246 relationship, and origin of the ferromagnetic minerals. We found that the Erawandoo Hill



247 conglomerate matrix contains abundant secondary hematite and the Erawandoo  
248 conglomerate and cobble conglomerate clasts contain predominantly iron sulfides and  
249 relatively few iron oxide grains (Fig. 4). WDS demonstrates that these sulfides are  
250 ferromagnetic monoclinic pyrrhotite and the nonmagnetic minerals pyrite, pentlandite  
251 and chalcopyrite (Fig. 4). Iron oxides in the Erawandoo Hill conglomerate are mainly in  
252 the form of FeOOH (including goethite) and hematite, whereas the cobble conglomerates  
253 contained hematite and magnetite grains.

254

255 *3.5. Summary of ferromagnetic mineralogy.* Collectively, our data show that the  
256 ferromagnetic minerals in the monzogranite and dolerite are dominantly iron oxides  
257 (mainly magnetite and goethite, with a secondary contribution from hematite), quartz  
258 clasts in the pebble and cobble conglomerates contain dominantly pyrrhotite with a  
259 secondary contribution from goethite and hematite and minor magnetite, and the  
260 quartzites and conglomerate matrices contain dominantly hematite, goethite, and  
261 pyrrhotite. Our observations of the cobble conglomerate mineralogy differ from those of  
262 Tarduno and Cottrell (2013), who inferred from high-temperature susceptibility data that  
263 their cobbles contain dominantly magnetite. Our data demonstrate that such  
264 measurements can obscure the presence of pyrrhotite and overemphasize the presence of  
265 magnetite due to oxidation of sulfides during the heating experiment.

266

## 267 **4. Paleomagnetism and geochronology**

### 268 *4.1. Overview*

269 In the field, we sampled oriented blocks using magnetic and sun compasses.  
270 Later at MIT, we drilled 25 mm-diameter cores (for all samples but most cobble  
271 conglomerates and the Erawandoo Hill pebble conglomerates), 12-mm diameter cores  
272 (from most of the cobble conglomerates), and microsampled mm-scale chips using a low-  
273 speed saw and hand drill (for the Erawandoo Hill pebble conglomerate). We named our  
274 samples after the field site at which they were acquired, followed by a letter and/or  
275 number for sites yielding multiple samples. To assess reproducibility, we often analyzed  
276 multiple subsamples from each of these samples; the names of these subsamples have a  
277 suffix consisting of a period followed by the subsample number.

278 We subjected most samples to stepwise alternating field (AF) demagnetization up  
279 to 10 mT. We then thermally demagnetized all subsamples up to peak temperatures  
280 ranging up to 680°C and measured their moments with a 2G Enterprises SRM 755  
281 equipped with an automatic sample handling system (Kirschvink et al., 2008) in the MIT  
282 Paleomagnetism Laboratory (demagnetization data are provided in the SM). Natural  
283 remanent magnetization (NRM) components were estimated using principal component  
284 analysis (Kirschvink, 1980) (Table S2).

285 AF demagnetization sometimes isolated low coercivity (LC) components.  
286 Subsequent thermal demagnetization often isolated additional components at low  
287 temperatures (LT), sometimes followed by origin-trending high temperature (HT)  
288 components. Occasionally, samples contained one or two additional medium temperature  
289 (MT) components, while many samples (particularly the cobbles) contained no coherent  
290 origin-trending HT component. Unless noted otherwise, magnetization directions are  
291 reported in geographic (i.e., in situ) coordinates rather than bedding-corrected  
292 coordinates. See SM for more details about how components were named and identified.

293 We note that only six samples (monzogranite sample D189, quartzite samples  
294 BC5 and BCB9, and three cobbles from sites W025 and W026) showed compelling  
295 evidence for lightning remagnetization, as indicated by anomalously high magnetizations  
296 (typically two orders of magnitude greater than surrounding rocks of similar lithology),  
297 single-component linear demagnetization trends, and anomalous magnetization  
298 directions. One of these parent sites (W025) also showed evidence for a lightning strike  
299 anomaly as indicated by deflection of a magnetic compass needle.

300

#### 301 4.2. Dolerite baked contact tests

302 A west-northwest trending dolerite dyke crosscuts interbedded conglomerate,  
303 quartzite, and siltstone about 200 m northeast of Erawandoo Hill (Fig. 1). The exposed  
304 portion of the dyke is ~250 m long and has a half-width,  $r_{dyke}$ , of ~5 m. It exhibits no  
305 evidence of deformation and cuts across fold structures and Proterozoic sedimentary  
306 rocks. The dyke previously has been correlated with the ~1070 Ma Warakurna LIP  
307 (Spaggiari, 2007b), an extensive series of intrusions, dykes, and volcanic rocks in central  
308 and Western Australia (Wingate et al., 2004) (Fig. 5A). Our U-Pb isotope dilution

309 thermal ionization mass spectrometry zircon weighted mean  $^{207}\text{Pb}/^{206}\text{Pb}$  date of  $1078.4 \pm$   
310  $3.4/4.4/6.6$  Ma from the dolerite (Fig. 5B and SM) confirms the dyke's association with  
311 the Warakurna LIP.

312 We conducted baked contact tests at three locations (sites BC, BCB, and D154)  
313 distributed along the strike of this and an adjacent dyke to establish the remagnetization  
314 history since 1078 Ma (Fig. 1 and 6A). At each site, samples were acquired of the dyke  
315 and from quartzitic country rock at progressively larger distances from the dyke.  
316 Thermal diffusion calculations indicate that a basaltic sheet dyke should heat intruded  
317 silicate country rock to  $\sim 530\text{-}580^\circ\text{C}$ ,  $\sim 350^\circ\text{C}$ , and  $\sim 170^\circ\text{C}$  at distances of 1.2, 2, and 4  
318 dyke radii from the dyke center assuming purely conductive heat transport [see Table 2 of  
319 Jaeger (1964)]. Therefore, given the peak unblocking temperatures observed for the  
320 country rocks (see below), we expect that samples at distances of  $<\sim 1.2 r_{dyke}$ , between  
321  $\sim 1.2$  and  $\sim 3 r_{dyke}$ , and  $>\sim 3 r_{dyke}$  should lie in the fully remagnetized, partially  
322 remagnetized, and weakly baked zones.

323 We found that individual unweathered dyke samples from the three sites typically  
324 contained two but sometimes up to five NRM components (Fig. 6B-F). LT components  
325 are directionally clustered with a mean direction close to the present geomagnetic field  
326 (Figs. 6 and S6). Nearly all samples contained a consistently-oriented, origin-trending  
327 HT component that unblocked between  $100\text{-}440^\circ\text{C}$  and  $530\text{-}580^\circ\text{C}$ , sometimes with a  
328 small remanence (almost always  $<5\%$  of NRM) persisting above  $580^\circ\text{C}$ . The peak  
329 unblocking temperature of the HT component along with our rock magnetic data (Section  
330 3) indicate it is carried primarily by magnetite, with a small contribution from hematite.  
331 Because the HT directions carried by both minerals are indistinguishable, it is likely that  
332 the hematite was produced by oxidation of magnetite during or soon after emplacement.  
333 A small number of samples (i.e., BC0.1, Dol5.1 and Dol5.2) exhibited a weak reversed  
334 component above  $540^\circ\text{C}$  that may be a self-reversal associated with martite [e.g.,  
335 Swanson-Hysell et al. (2011)]. The dyke mean HT direction (declination  $19.1^\circ$ ,  
336 inclination  $47.6^\circ$ ,  $\alpha_{95} = 8.3^\circ$ , and estimated Fisher precision parameter  $k = 8.7$ ) has a  
337 virtual geomagnetic pole (VGP) located at latitude  $\theta = 31.7^\circ$  N and longitude  $\varphi = 136.6^\circ$   
338 E (95% confidence ellipse with semiaxes of  $dp = 8.8^\circ$  and  $dm = 13.5^\circ$ ). Assuming a  
339 typical rock thermal diffusivity of  $D = 10^{-6} \text{ m}^2\text{s}^{-1}$ , the dyke should have required a time  $t$

340  $\approx r_{dyke}^2/D \approx 1$  y to diffusively cool from the magnetite Curie point to ambient  
341 temperatures, meaning that its VGP should not average typical secular variation. Allowing  
342 for this, the pole is likely associated with the dyke VGP is broadly similar to that of  
343 Warakurna LIP rocks (e.g., the Bangemall basin dolerite sills:  $\theta = 33.8^\circ$  N and longitude  
344  $\varphi = 95.0^\circ$  E, 95% confidence interval  $A_{95} = 8.3^\circ$ , modified quality criterion AV value = 6  
345 out of 6) (Wingate et al., 2004) (Fig. 6F).

346 Individual country rock samples near the dolerite at the three sites contained  
347 between one and three NRM components. Although the demagnetization trends are  
348 noisy for many samples, multiple subsamples from individual cores usually yield similar  
349 components (e.g., cores BCB4 and D154i). Most samples contained a LT component  
350 removed by 80-440°C depending on the sample. The LT components collectively are  
351 scattered but have a mean direction within error of the present geomagnetic field,  
352 suggesting a recent origin (Fig. S6). Most samples contained an origin-trending HT  
353 component with maximum unblocking temperatures ranging from 225 to 580°C (and  
354 usually >500°C). The combined mean HT directions for each of the fully baked, partially  
355 baked and weakly baked zones for the three sites (Table S2) are essentially  
356 indistinguishable from the dolerite HT mean (Fig. 6F), indicating failed baked contact  
357 tests. The country rock, even at the maximum sampling distance of  $7.8 r_{dyke}$ , is  
358 magnetized in the direction of the dyke. Because this is far beyond the expected  
359 conductive thermal remagnetization zone, it suggests that regional-scale thermal and/or  
360 chemical remagnetization affected the Erawandoo Hill as a result of the Warakurna LIP.

361

#### 362 *4.3. Monzogranite and quartzitic country rock*

363 Further evidence for regional-scale remagnetization is provided by our analyses of  
364 monzogranite and country rock from 14 sites distal to the dyke. In particular, we  
365 analyzed the  $2654 \pm 7$  Ma monzogranite intruding supracrustal rocks ~3 km to the west-  
366 southwest from Erawandoo Hill (“The Blob”) (Wilde and Pidgeon, 1990) (D182-D189,  
367 Blob4, and Blob5) and quartzites and quartz pebble conglomerates (sites D192, D194,  
368 D195, and D196) located 0.8 to 2 km to the west of Erawandoo Hill (Fig. 1). Thermal  
369 diffusion calculations (Section 4.2) indicate that sites D194, D195, D196, along with fold  
370 site D197 (see Section 4.4), should be within the partial to full thermal remagnetization

371 zone of the monzogranite Blob and therefore constitute another large-scale baked contact  
372 test for remagnetization since 2654 Ma.

373 We found that most monzogranite samples contained an LT component removed  
374 by 80-290°C that is indistinguishable from that of the present geomagnetic field (Figs. 7  
375 and S6). This common direction and the abundance of goethite in some of these samples  
376 (Section 3) indicate that the LT component likely was produced by recent oxidative  
377 weathering. Nearly all samples also contained an HT component that unblocked from the  
378 end of the LT component up to a maximum temperature of nearly 580°C (Fig. 7). The  
379 mean HT direction is indistinguishable from the Warakurna LIP local paleofield direction  
380 (Section 4.2).

381 We found that most quartzitic rocks also carried LT components that thermally  
382 demagnetized up to 80-360°C. Although collectively scattered, their mean is within error  
383 of the present geomagnetic field, consistent with a recent origin (Fig. S6). Sites D192,  
384 D194, D195, and D197 also contain an HT component (removed from the end of the LT  
385 component usually up to a maximum temperature of 290 to 360°C, but reaching 520°C  
386 for sample D194c) with a mean direction near the Warakurna LIP local paleofield  
387 direction (Figs. 7 and S6).

388

#### 389 *4.4. Fold tests*

390 We identified two meter-scale folds in metamorphosed quartz pebble  
391 conglomerates 0.7 km northeast (D102) and 2.0 km west (D197) of Erawandoo Hill  
392 (Figs. 1 and 8). At site D102, there is a southeast verging fault propagation fold with 10  
393 cm scale parasitic folding superimposed on the meter-scale hinge zone. The fault bend is  
394 not deformed, but the entire structure is rotated with the bedding (074/82) such that the  
395 fold hinge line is near-vertical. At site D197, there is a southeast-verging kink band  
396 within beds with strike/dip = 234/62. The steeply-plunging fold axes within strongly  
397 sheared beds suggest that the meter-scale folding is older than the map-scale regional  
398 tilting of the meta conglomerates and sandstones. At a minimum, the cross-cutting  
399 relationship requires the meter-scale folding to be older than intrusion of the dolerite  
400 dyke. At both sites, oriented samples were collected from a variety of orientations  
401 around major and parasitic fold hinges.

402 We found that most samples from site D102 have scattered LT components that  
403 unblocked up to ~200-275°C with a mean direction within error of the present  
404 geomagnetic field (Figs. 8 and S6). Given this common direction and the abundance of  
405 goethite in these samples (Section 3), the LT components are likely of recent origin. All  
406 samples but D102c also contained an origin-trending HT component blocked up to 325-  
407 350°C. The HT directions are equally scattered in both in situ (i.e., geographic) and  
408 bedding-tilt coordinates (ratio of estimated Fisher precision parameters with and without  
409 tilt correction  $k_{tilt}/k_{geo} = 1.0$ ). Therefore, the fold test at this site is inconclusive (does not  
410 pass at the 95% confidence interval).

411 We found that site D197 samples exhibited typically weak and scattered LT  
412 components that unblocked up to 100-300°C (Figs. 8 and S6). All samples contained a  
413 dominant MT component that unblocked up to 325-350°C and many samples also  
414 contained a weak HT component that unblocked up to 640°C (Figs. 8 and S7). The MT  
415 components become more scattered after bedding tilt-correction ( $k_{tilt}/k_{geo} = 0.46$ ) and  
416 therefore fail the fold test. Furthermore, the MT directions in geographic coordinates are  
417 well-clustered and within error of the local mean Warakurna LIP paleofield direction  
418 (Section 4.3). The fold test for the HT directions is inconclusive ( $k_{tilt}/k_{geo} = 1.20$ , such  
419 that it does not pass the fold test at the 95% confidence interval); given that the HT mean  
420 direction is within error of the present geomagnetic field direction and is carried by  
421 hematite [as required by its peak unblocking temperature and supported by our rock  
422 magnetic data (Section 3)], it probably originated during recent oxidative weathering.

423

#### 424 4.5. Conglomerate tests

##### 425 4.5.1. Erawandoo Hill pebble conglomerate

426 We conducted three paleomagnetic conglomerate tests on mm-diameter quartz  
427 clasts from three blocks sampled from three sites (EHJH5, EHJH6, and EHJH7) in the  
428 Erawandoo Hill Hadean zircon-bearing pebble conglomerate (Fig 1). A total of 55  
429 oriented clasts and 29 oriented bulk matrix samples were extracted from each block using  
430 nonmagnetic dental tools and saws. Seven of these clasts were further subdivided into a  
431 total of 21 subsamples to test whether the clast magnetization in the clasts is

432 unidirectionally oriented. The samples were mounted on 25 mm diameter nonmagnetic  
433 GE 124 quartz disks using nonmagnetic adhesives.

434 We found that most samples have an LT component that thermally demagnetized  
435 by ~150-250°C (Fig. 9). The LT components in EHJH5 have a mean direction within  
436 error of the present local geomagnetic field and therefore likely originated recently (Fig.  
437 S6). Many samples also have an origin-trending HT component unblocked from the end  
438 of the LT component up to between 325-350°C (and persisting up to at least 500°C for  
439 one sample). Many other samples (particularly from EHJH6) never reached origin-  
440 trending trajectories due the acquisition of spurious remanence during demagnetization.  
441 The distribution of HT components that were inferred from EHJH6 extends  
442 asymmetrically toward the block's mean LT direction, suggesting that the two  
443 components are carried by grains with overlapping blocking temperatures. This may also  
444 explain why the LT components from EHJH7 differ in direction and are within error of  
445 the HT direction for this block.

446 The stable HT components isolated from clast and matrix samples are dominantly  
447 unidirectionally oriented within each block. In particular, the 31 clasts from EHJH5 and  
448 10 clasts from EHJH6 are nonrandomly magnetized at >99% confidence (resultant  
449 vectors  $R = 28.2$  and  $6.9$ , respectively), while the 2 clasts from EHJH7 are nonrandomly  
450 magnetized at 95% confidence. This result indicates that the characteristic magnetization  
451 of all three blocks was acquired after deposition of the conglomerate at 3.0-2.65 Ga. The  
452 grand HT mean for the three blocks is indistinguishable from the local Warakurna LIP  
453 paleofield direction, suggesting remagnetization by this ~1070 Ma igneous event.  
454 Although the mean directions of the three blocks are distinct to >95% confidence from  
455 the Warakurna LIP direction, all subsamples from each block are from just several cm of  
456 stratigraphy (and so the block means are unlikely to completely average secular variation)  
457 and all share the same orientation of the parent block (and so are subject to systematic  
458 errors associated with orienting the parent block and deviation of the block orientation  
459 from that of the local bedding).

460

461 *4.5.2. Cobble conglomerate*

462 Conglomerates containing large (0.5-30 cm long) cobbles outcrop ~500 m  
463 northwest of Erawandoo Hill (Fig. 1). These cobbles are elongated and metamorphically  
464 flattened and composed mainly of quartz, chert and quartzite and are supported in a sandy  
465 matrix. We sampled 35 cobbles at 9 sites distributed 1.6 km along strike in the cobble  
466 beds (sites D107-D112, D192, W025, and W026), with the latter two sites located within  
467 ~37 m of the samples of Tarduno and Cottrell (2013). This yielded enough samples for  
468 three separate conglomerate tests: at sites D111, D112, and a test combining adjacent  
469 sites W025 and W026. At each of these sites, the cobbles were sampled at most <5 m  
470 apart to ensure that they have similar depositional ages, metamorphic histories, and have  
471 not experienced within-site differential rotation (whereas the samples of Tarduno and  
472 Cottrell (2013) were acquired over a ~200 m area). Our samples generally are from the  
473 same lithologic population but are probably not from the very same beds as those  
474 sampled by Tarduno and Cottrell (2013). Detrital zircon dates (Grange et al., 2010) show  
475 these conglomerates were probably deposited after 1.7 Ga (and perhaps after 1.22 Ga).

476 At MIT, we drilled 13 mm or 25 mm diameter cores through the centers of each  
477 cobble. We then sliced the cores and acquired individual subsamples from near the  
478 center of each core and away from any apparent fractures and secondary alteration. For  
479 most cobbles, we obtained two subsamples to test for homogeneity of NRM. The  
480 samples from the 13 mm cores were mounted on 25 mm diameter nonmagnetic GE 124  
481 quartz disks using double-sided tape. The disk mounts were regularly cleaned and their  
482 moments measured after each demagnetization step to ensure that their moments  
483 remained no more than 5% of those of the samples.

484 Unlike other Jack Hills samples analyzed in this study, the majority of cobbles  
485 exhibited highly unstable demagnetization behavior (Figs. 10 and S9). In most cases, the  
486 little modestly stable demagnetization behavior observed was in the form of LC (removed  
487 by <10 mT) and/or LT components (unblocked by 100-275°C) that are collectively  
488 scattered (Figs. 10A and S6). After removal of this component, most cobbles exhibited  
489 large directional changes, often without decaying in moment or ever settling to an origin-  
490 trending direction. Furthermore, subsamples from these cobbles usually exhibited  
491 strikingly nonhomogeneous NRM directions and demagnetization trends (Fig. 10).



492 As a result, we identified origin-trending HT components from only 22 out of 61  
493 subsamples (15 out of 35 cobbles). Even for these 22 samples, only 14 samples (7  
494 cobbles) demonstrated homogenous intra-cobble HT components (Table S2). No such  
495 stably magnetized cobbles were identified from sites D111 and D112, while only 4 such  
496 cobbles were identified from the combined W025 and W026 (Fig. S8). However, the  
497 significance of even these four samples is highly suspect: three are likely lightning-  
498 remagnetized (they have only a single magnetization component, have the strongest  
499 NRM intensities among samples at these sites, and a magnetic anomaly was observed at  
500 near the sampling site from magnetic compass field observations), while the HT  
501 component of the fourth is carried by hematite and so is likely secondary. With a single  
502 exception (cobble W025k), all of the rest of the cobbles with HT components were  
503 completely demagnetized by 350°C. These observed low unblocking temperatures are  
504 consistent with the dominance of pyrrhotite and goethite as indicated by our petrographic  
505 and rock magnetic data (Section 3). Note that we observed no systematic differences in  
506 cobble demagnetization with respect to cobble size, shape, sampling location, or core  
507 size.

508 Overall, these results are very different from those reported by Tarduno and  
509 Cottrell (2013), who reported highly stable, origin-trending characteristic high-  
510 temperature NRM components that unblocked from ~545°C to 570-580°C in 27 out of 28  
511 cobbles and observed homogenous NRM components within the 3 individual cobbles that  
512 they subsampled. We also do not see any evidence of a shallow southeast overprint  
513 observed in 20% of the samples reported by Tarduno and Cottrell (2013) (Fig. S6).

514

## 515 **5. Implications**

516 We find that the main remanence carrier in the Jack Hills quartzitic sediments is  
517 the low blocking temperature mineral pyrrhotite and, to a lesser extent, goethite.  
518 Therefore, with a few exceptions, we are only able to assess the remagnetization history  
519 in the sediments up to temperatures of ~330°C (Table S3). Most of the remanence in the  
520 few sedimentary samples with higher NRM unblocking temperatures is carried by  
521 hematite, is oriented in the direction of the present local geomagnetic field, and is  
522 therefore likely of recent origin by oxidative weathering. On the other hand, the igneous

523 rocks (monzogranite and dolerite) and several quartzitic samples contain abundant  
524 magnetite and record remagnetization up to unblocking temperatures of 580°C (Table  
525 S3).

526 All three of our Erawandoo Hill pebble conglomerate tests failed, indicating  
527 complete remagnetization up to the maximum observed unblocking temperatures of 335-  
528 500°C (Table S3). The mean remagnetization directions are close to that of a nearby  
529 1078 Ma dolerite dyke and of the local geomagnetic field during the contemporaneous  
530 ~1070 Ma Warakurna LIP.

531 Furthermore, we found that clasts from the cobble conglomerates behave  
532 extremely unstably during laboratory demagnetization with blocking temperatures almost  
533 exclusively <350°C, nonlinear magnetization trends that often do not reach origin-  
534 trending directions, and nonunidirectional magnetization directions within single cobbles.  
535 Such inhomogeneous and low-stability NRM can be produced by fine-scale aqueous  
536 alteration, weathering, and viscous remagnetization and invalidates the use of a  
537 conglomerate test for these samples. Furthermore, given the low unblocking  
538 temperatures of the cobble NRM, if these rocks experienced the same 350°C-500°C  
539 greenschist metamorphic event that affected the Erawandoo Hill rocks (Section 2), this  
540 would require that the cobbles' NRM postdates deposition.

541 Our cobble conglomerate test results contrast starkly with those of Tarduno and  
542 Cottrell (2013), who argued that the magnetizations of their clasts are dominantly carried  
543 by magnetite and who reported stable, origin-trending components that unblocked  
544 between 540 and 600°C. The reasons for the great differences in ferromagnetic  
545 mineralogy and NRM between our two studies are unknown. It is conceivable that the  
546 two sample suites are simply lithologically distinct at the microscale (even though they  
547 appear similar at hand sample and outcrop scale). A second possibility is that the more  
548 stable NRM observed in Tarduno and Cottrell (2013)'s samples is the product of  
549 lightning-remagnetization. However, both of these explanation are unsatisfying because  
550 they would require that by improbably low chance our samples suites are very different:  
551 among our 35 cobbles, we only observe a single cobble (D107g) with an NRM  
552 apparently carried by magnetite and three cobbles carrying highly stable NRM  
553 characteristic of lightning remagnetization, whereas all 28 of Tarduno and Cottrell

554 (2013)'s cobbles have NRMs apparently dominated by magnetite. A third possibility is  
555 that our two sample suites have similar NRMs, but that subtle differences in laboratory  
556 methodology (i.e., sample contamination or alteration during heating) led to major  
557 differences in demagnetization behavior. Regardless, as discussed above, even if the  
558 positive conglomerate test of Tarduno and Cottrell (2013) is accepted, it would only  
559 confidently exclude remagnetization since 1.7 Ga (and possibly post-1.22 Ga), not since  
560 the Paleoproterozoic.

561 Our fold tests failed or were inconclusive, suggesting that the host rocks were  
562 likely remagnetized after the folding events. In particular, the site D197 rocks are  
563 remagnetized in the direction of the ~1.1 Ga Warakurna LIP up to unblocking  
564 temperatures of 350°C (Table S3). Associated with a local Warakurna dyke, all of our  
565 three baked contact tests were negative, with quartzite more than three dyke radii from  
566 the dyke center magnetized in the dyke's direction up to unblocking temperatures of at  
567 least 560-580°C (Table S3). Furthermore, we have found that Erawandoo Hill pebble  
568 conglomerate samples from 0.2 km away, and even monzogranite up to at least 3 km  
569 away, are nearly completely magnetized in the dyke's direction up to unblocking  
570 temperatures of 580°C.

571 With the exception of poles from the mid-Neoproterozoic (~770 Ma), the  
572 dyke/Warakurna direction is distinct at >95% confidence from poles younger than 1070  
573 Ma along Australia's apparent polar wander path (Swanson-Hysell et al., 2012; Torsvik  
574 et al., 2012), indicating that the remagnetization process was likely complete soon after  
575 dyke emplacement and is unlikely to be the product of a subsequent events unrelated to  
576 dyke emplacement. However, the peak temperature expected for country rock  
577 experiencing a purely thermal diffusive pulse from the intrusion of such a small dyke is  
578 insufficient to remagnetize rocks at such distal sites. We propose two alternative possible  
579 scenarios to account for these observations.

580 A first possibility is that regional-scale heating and/or hydrothermal alteration was  
581 generated by the magmatic activity from the Warakurna LIP, which is thought to have  
582 extended over much of west Australia at this time as the near-surface manifestation of a  
583 >1500 km diameter hot mantle plume head (Wingate et al., 2004). Numerous other  
584 dykes attributed to the Warakurna event have been identified throughout the Jack Hills

585 (Spaggiari, 2007b) and northwest Yilgarn craton (Wingate et al., 2004). The fact that the  
586 monzogranite and some quartzitic rocks contain a magnetite-bearing HT component  
587 magnetized in the Warakurna LIP direction up to unblocking temperatures of 580°C  
588 would seem to imply a total thermoremanent magnetization (TRM) overprint from  
589 heating to at least 580°C. However, such a high temperature appears to conflict with Ti-  
590 in-quartz and monazite-xenotime thermometry, which suggest peak metamorphic  
591 temperatures of ~346-487°C. An alternative is that metamorphic temperatures from the  
592 Warakurna event were less than 580°C and the monzogranite appears completely  
593 remagnetized due to the presence of multidomain grains with distributed unblocking  
594 temperatures approaching the magnetite Curie point (Dunlop and Özdemir, 1997).  
595 However, this would not readily explain the complete remagnetization of the small  
596 number of magnetite-bearing quartzitic rocks. A second alternative is that the Jack Hills  
597 was overprinted by a crystallization remanent magnetization (CRM) associated with  
598 aqueous alteration and metasomatism. In fact, it has been proposed that the presence of  
599 numerous epigenetic mineral deposits (including sulfide ores) throughout the Warakurna  
600 LIP region reflects a giant hydrothermal system at 1070 Ma (Pirajno, 2004; Wingate et  
601 al., 2004). Dissolution and reprecipitation of pyrrhotite and other sulfides is a common  
602 consequence of metasomatic processes in sediments (Hall, 1986), which could explain  
603 our observation that pyrrhotite is the dominant NRM carrier in our quartzite and  
604 conglomerate samples. In such a case, one cannot exclude the possibility that some  
605 inclusions armored within zircons might have escaped being aqueously remagnetized.  
606 However, this aqueous remagnetization scenario cannot readily account for the  
607 remagnetization of the monzogranite, whose characteristic NRM is dominated by  
608 magnetite.

609         A second scenario is that the local geomagnetic field direction at 2650 Ma was  
610 similar to that at 1070 Ma, such that intrusion of the monzogranite at the earlier time  
611 remagnetized much of the west-central Jack Hills in a direction coincidentally close to  
612 that of the dyke. We cannot exclude this scenario because the apparent polar wander path  
613 of the Narryer terrane is poorly constrained prior to 2418 Ma (Schmidt, 2014; Smirnov et  
614 al., 2013; Veikkolainen et al., 2014).

615

616 **6. Conclusions**

617 Our 11 field tests using 277 total subsamples from the area surrounding the Jack  
618 Hills Hadean-zircon bearing rocks at Erawandoo Hill yielded either negative outcomes,  
619 indicating complete remagnetization, or inconclusive results due to a lack of stable  
620 magnetization. These results include the first conglomerate tests directly on the  
621 Erawandoo Hill conglomerate. The bulk of the available evidence indicates that the  
622 Erawandoo Hill Hadean-zircon bearing pebble conglomerates, although largely free of  
623 the effects of lightning strikes, were pervasively remagnetized up to unblocking  
624 temperatures of at least 330°C, and some nearby quartzites up to 580°C, either by  
625 emplacement of the Warakurna LIP at 1070 Ma and/or by the intrusion of monzogranite  
626 at 2650 Ma.

627 It is unclear whether the remagnetization process that affected the Jack Hills rocks  
628 was a TRM from heating or a CRM due to aqueous alteration. In the case of a TRM, the  
629 peak 580°C unblocking temperatures of the Warakurna/dyke direction in most of the  
630 monzogranite samples and in selected quartzitic sediments may imply total thermal  
631 remagnetization of magnetite-bearing zircons in these and nearby rocks. However, such  
632 temperatures appear to conflict with some mineral thermometry estimates and therefore  
633 support at least some chemical remagnetization. In any case, even if it could eventually  
634 be established that the zircons have not been remagnetized completely since deposition at  
635 2.65-3.05 Ga, the age of their magnetization would remain unconstrained for the missing  
636 0.35-1.45 billion year rock record following their crystallization but predating the  
637 deposition of their host rocks.

638

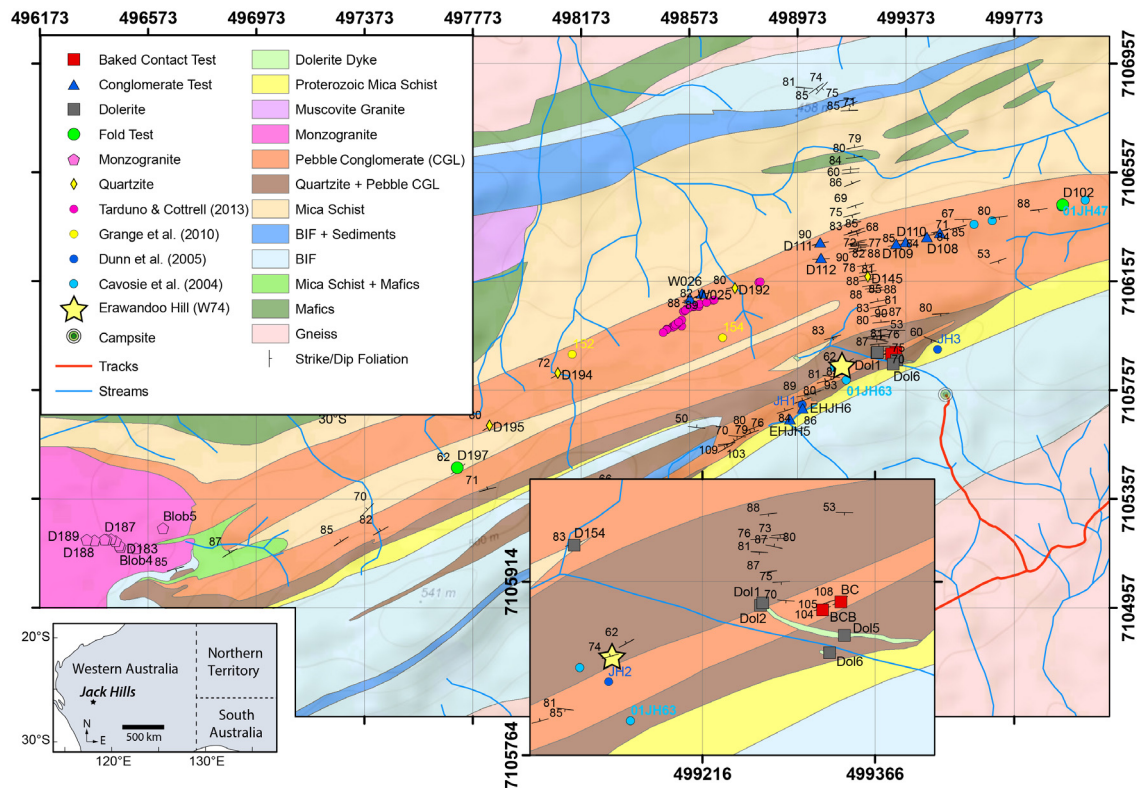
639 **Acknowledgements**

640 We thank S. Mojzsis for introducing us to the Jack Hills in 2001, the Geological Survey  
641 of Western Australia for access to the Jack Hills Geoheritage Reserve, the residents and  
642 goat of Beringarra Station for logistical help, Crosslands Resources for showing us their  
643 iron ore mine, M. Wingate and R. Pidgeon for helpful discussions and logistical  
644 assistance, and D. A. D. Evans for helpful discussions on polar wander. We also thank S.  
645 Ceballos, S. Bouma, and F. Hellman for assistance with magnetometry measurements, B.  
646 Carbone for administrative help, R. Bowens-Rubin for acquiring the EHJH5

647 measurements, and the NSF Early Concept Grants for Exploratory Research program for  
648 support.

649

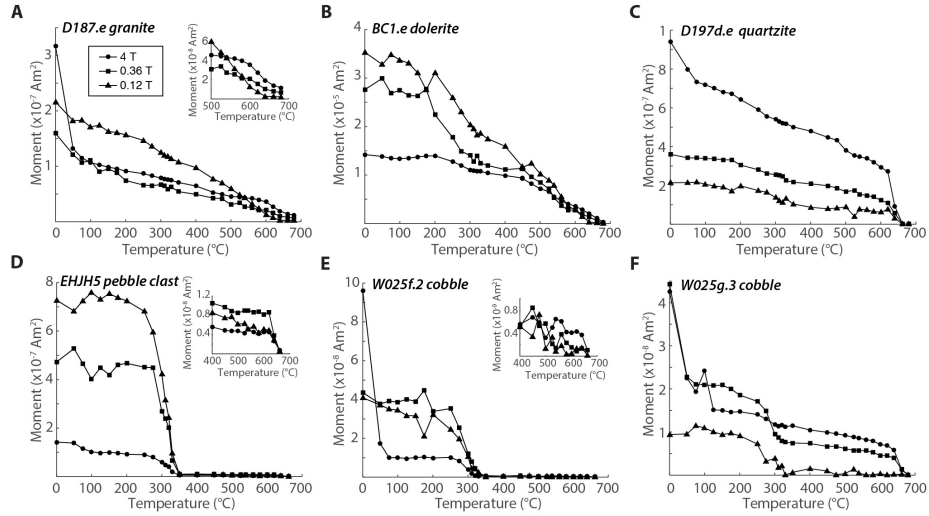
Figures



651

652 **Fig. 1.** Generalized geological map of the central-west Jack Hills after Spaggiari  
 653 (2007b). Inset at bottom left shows regional location in Western Australia. (A)  
 654 Overview of sampling area. Lithologies are denoted by light shaded colors. Our baked  
 655 contact, fold, and conglomerate test sites are noted. Yellow star denotes discovery site of  
 656 >4 Ga zircons (Erawandoo Hill, also known as W74). Locations of Proterozoic detrital  
 657 zircons sampled by Cavosie et al. (2004), Dunn et al. (2005), and Grange et al. (2010) are  
 658 denoted by small light blue, dark blue and yellow circles. Sampling localities for  
 659 individual cobbles sampled by Tarduno and Cottrell (2013) are shown by small magenta  
 660 circles. All geological contacts are estimated. Stratigraphic up direction is frequently  
 661 ambiguous within the quartzites and conglomerates, but is usually toward the southeast.  
 662 Magnetic declination was set to zero degrees; the estimated local declination was  $\sim 0.4^\circ$ .  
 663 Projection is with the Universal Transverse Mercator grid in the World Geodetic System  
 664 1984 standard. Spacing between contour lines (grey) is 50 m.

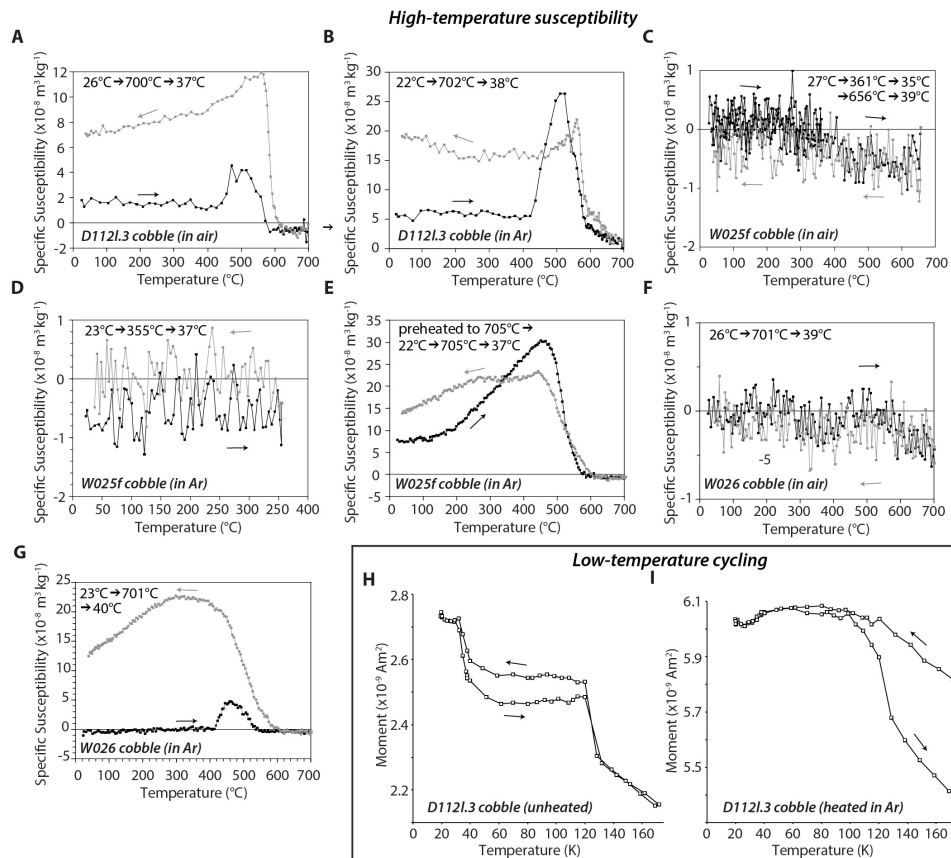
665



666  
 667  
 668  
 669  
 670  
 671  
 672  
 673  
 674  
 675  
 676

**Fig. 2.** Selected examples of thermal demagnetization of a three-component IRM produced by magnetizing the sample in a 4 T along the  $z$ -axis, followed by 0.36 T along the  $x$ -axis, and 0.12 T along the  $y$ -axis. Each plot contains curves showing the corresponding  $z$ - (circles),  $y$ - (squares), and  $x$ - (triangles) magnetization components. (A) Monzogranite sample D187.e. (B) Dolerite sample BC1.e. (C) Quartzitic fold test sample D197d.e. (D) Clast from Erawandoo Hill pebble conglomerate EHJH5c. (E) Clast from cobble conglomerate W025f.2. (F) Clast from cobble conglomerate W025g.3. See Fig. S2 for more examples of thermal demagnetization of three-axis IRM.

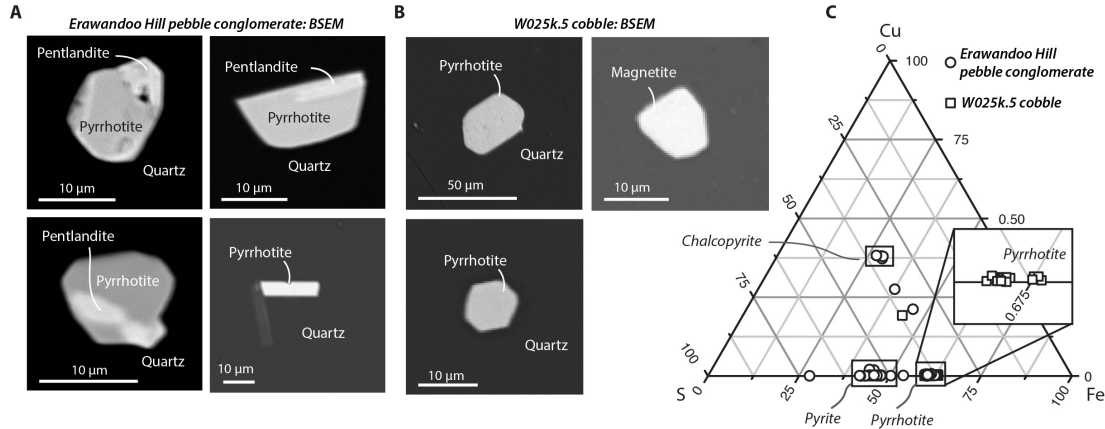




677  
 678 **Fig. 3.** High temperature susceptibility (A-G) and low temperature cycling of room  
 679 temperature saturation IRM measurements (H, I) on Jack Hills cobbles. (A) D1121.3  
 680 cycled in air up to 702°C. (B) D1121.3 cycled in Ar cycled up to 700°C. (C) W025f  
 681 cycled in air first to 361°C and then to 656°C. (D) W025f cycled in Ar up to 355°C. (E)  
 682 W025f cycled in Ar up to 705°C. Prior to these measurements, sample had been  
 683 previously heated in Ar up to 705°C (see Fig. S1D). (F) Cobble W026 cycled in air up to  
 684 701°C. (G) Cobble W026 cycled in Ar up to 701°C. (G) Cobble D1121.3 unheated. (H)  
 685 Cobble D1121.3 previously subjected to temperature-dependent susceptibility analyses in  
 686 Ar [see (B)]. See Fig. S1 for more examples of high-temperature susceptibility data.

687

688



689

690 **Fig. 4.** Electron microscopy of Jack Hills conglomerate clasts. (A) BSEM images of

691 iron sulfides in quartz clasts from the Erawandoo Hill pebble conglomerate. (B) BSEM

692 images of pyrrhotite and magnetite in quartz cobble sample W025k.5. (C) WDS

693 compositional analyses of sulfides in Erawandoo pebble conglomerate and W025k

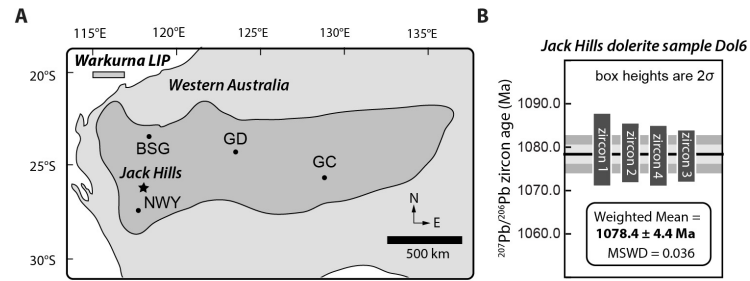
694 cobble. The observed ratios of Fe, S, and Cu indicate the presence of monoclinic

695 pyrrhotite, pyrite, and chalcopyrite. Inset shows magnification around pyrrhotite

696 composition; for clarity, measurements shown from only W025k.5.

697

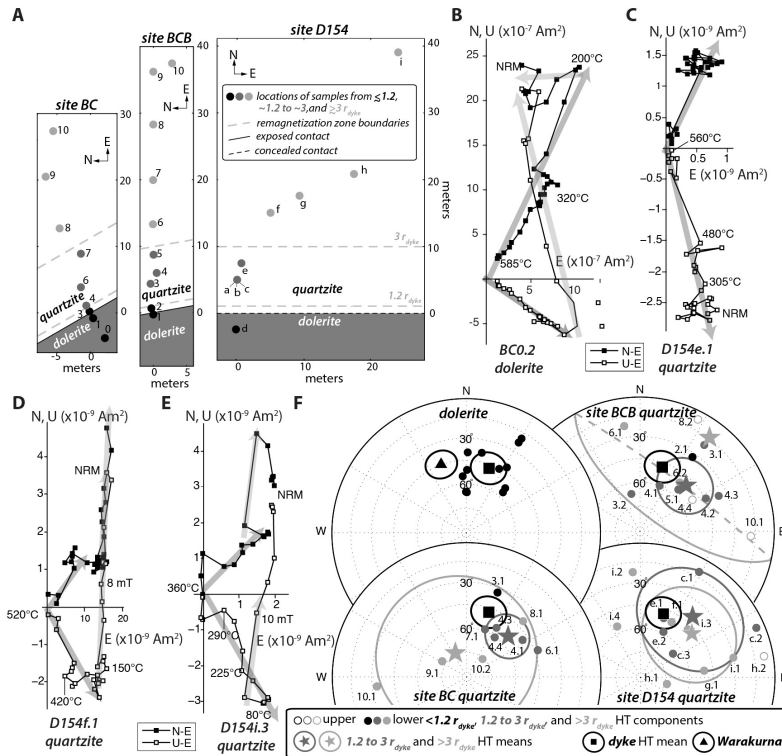
698



699  
 700 **Fig. 5.** (A) Geographic extent of the Warakurna LIP in west Australia, including its major  
 701 mafic sill and dyke intrusions and their published sensitive high-resolution ion  
 702 microprobe (SHRIMP) U-Pb dates ( $2\sigma$  uncertainties) from Wingate et al. (2004). BSG =  
 703 Western Bangemall Supergroup sills:  $1071 \pm 8$  Ma,  $1067 \pm 14$  Ma and  $1068 \pm 22$  Ma;  
 704 GC = Giles Complex:  $1073 \pm 5$  Ma and  $1058 \pm 14$  Ma; GD = Glenayle Dolerite:  $1063 \pm$   
 705  $21$  Ma and  $1068 \pm 20$  Ma; NWY = Northwest Yilgarn dykes:  $1075 \pm 10$  Ma. Star denotes  
 706 location of Jack Hills. See Wingate et al. (2004) for U-Pb radiometric age uncertainties,  
 707 methods, and references. (B) Date distribution plot for the analyzed zircons from dolerite  
 708 dyke adjacent to Erawandoo Hill in the Jack Hills. Vertical axis is measured  $^{207}\text{Pb}/^{206}\text{Pb}$   
 709 date; bar heights represent  $2\sigma$  analytical uncertainty of individual analyses. Shaded  
 710 horizontal bands and their width signify uncertainty in the weighted mean date at  $1\sigma$  and  
 711  $2\sigma$  levels. MSWD is mean square of weighted deviates. See SM for detailed U-Pb data  
 712 and interpretation.

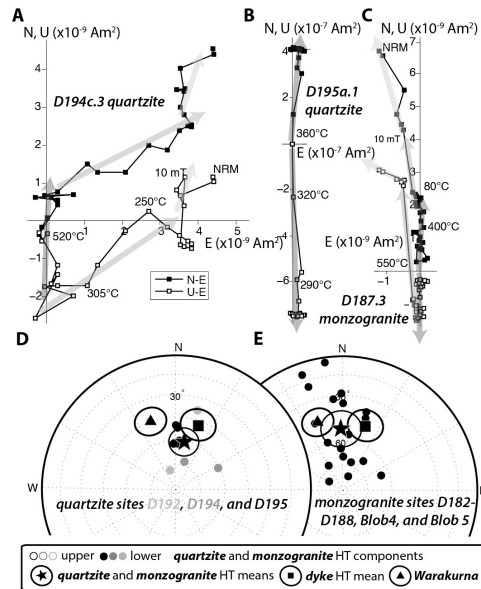
713

714

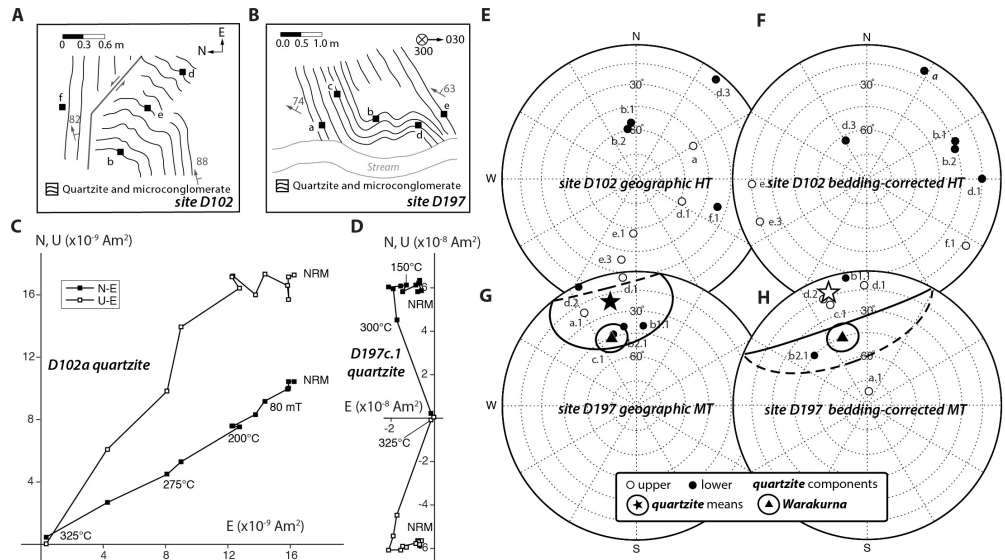


715  
 716 **Fig. 6.** Dolerite baked contact tests at sites BC, BCB, and D154. (A) Simplified maps  
 717 showing locations of dolerite and quartzitic country rock samples (circles) at each site.  
 718 The shade of each point corresponds to distance of sample from center of dyke and  
 719 dashed grey lines denote approximate boundaries of thermal remagnetization zones  
 720 assuming simple thermal diffusion (see text). Solid and dashed black lines denote  
 721 observed and concealed contact, respectively, between dolerite and quartzite. (B-E)  
 722 Two-dimensional projection of the endpoint of the NRM vector during AF and thermal  
 723 demagnetization in geographic coordinates for dolerite sample D011.1 (B) and quartzitic  
 724 samples D154e.1 (C), and D154f.1 (D), and D154i.3 (E). Closed and open symbols  
 725 represent end points of magnetization projected onto north-east (N-E) and up-east (U-E)  
 726 planes, respectively. Peak AC fields and temperatures for selected AF and thermal  
 727 demagnetization steps are labeled. Also shown are LT (lighter arrows) and HT (dark  
 728 arrows) components. (F) Equal area stereonet showing directions of HT components  
 729 from the dolerite at all three sites (top left) and quartzitic rocks from sites BCB (upper  
 730 right), site BC (lower left), and site D154 (lower right). Open and closed symbols  
 731 represent upper and lower hemispheres. Also shown are Fisher HT mean directions and

732 associated 95% confidence ellipse from dolerite (squares) and country rock samples from  
 733 outer two thermal remagnetization zones (dark and light gray stars) at sites BCB, BC, and  
 734 D154. Triangle and associated ellipse denotes local paleomagnetic field direction and  
 735 95% confidence interval for mean pole for Bangemall Supergroup sills (part of  
 736 Warakurna LIP) (Wingate et al., 2002).  
 737



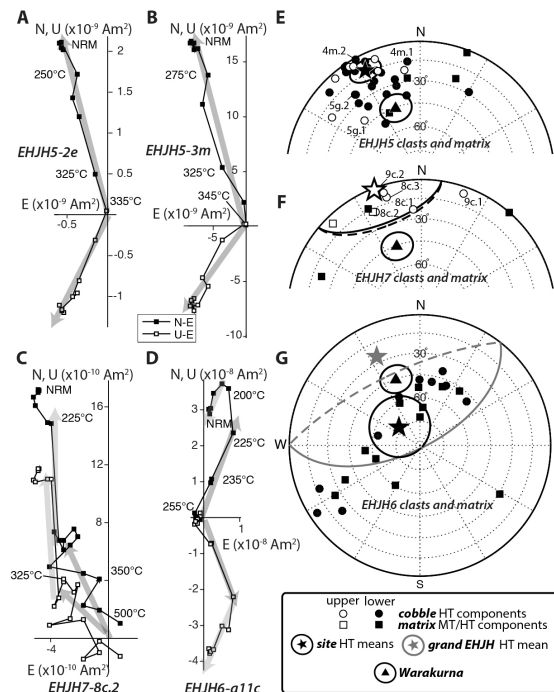
738  
 739 **Fig. 7.** Paleomagnetism of monzogranite and quartzite. Two-dimensional projection of  
 740 the endpoint of the NRM vector during AF and thermal demagnetization in geographic  
 741 coordinates for quartzitic samples D194c.3 (A) and D195a.1 (B) and monzogranite  
 742 sample D187.3 (C). Closed and open symbols represent end points of magnetization  
 743 projected onto north-east (N-E) and up-east (U-E) planes, respectively. Temperatures for  
 744 selected thermal demagnetization steps are labeled. Also shown are LC (lightest arrows),  
 745 LT (intermediate shaded arrows) and HT (dark arrows) components. (D, E) Equal area  
 746 stereonet showing directions of HT components from the quartzite sites D192, D194, and  
 747 D195 (D) and monzogranite sites D182-D188, Blob4 and Blob5 (E). Open and closed  
 748 symbols represent upper and lower hemispheres. Stars, square and triangle with  
 749 associated ellipses denote monzogranite and quartzite HT means, dolerite HT mean (Fig.  
 750 6F), and local paleomagnetic field direction for mean pole for Bangemall Supergroup  
 751 sills (part of Warakurna LIP) (Wingate et al., 2002) with 95% confidence intervals,  
 752 respectively.  
 753



754

755 **Fig. 8.** Fold tests at sites D102 and D197. (A, B) Simplified map of D102 (A) and D197  
 756 (B) sites showing sample location (squares), bedding planes (curvy lines), field  
 757 measurements of bedding strikes (hatched arrows) and dips (numbers), sinistral fault  
 758 [grey line with grey arrows in (A)] and streambed [light grey lines in (B)]. Scale bars are  
 759 0.6 m (A) and 1.0 m (B). Compasses denote geographic north and east (A) and  
 760 declinations  $30^\circ$  and  $300^\circ$  (B). (C, D) Two-dimensional projection of the endpoint of the  
 761 NRM vector during AF and thermal demagnetization in geographic coordinates for  
 762 quartzitic samples D102a.1 (C), and D197c.1 (D). Closed and open symbols represent  
 763 end points of magnetization projected onto north-east (N-E) and up-east (U-E) planes,  
 764 respectively. Peak AC fields and temperatures for selected AF and thermal  
 765 demagnetization steps are labeled. Also shown are LT components (lighter arrows) and  
 766 HT (for D102a) and MT (for D197c.1) components (dark arrows). (E-H) Equal area  
 767 stereonet showing directions of HT components from the quartzitic site D102 in  
 768 geographic (E) and bedding-corrected coordinates (F) and MT components from  
 769 quartzitic site D197 in geographic (G) and bedding-corrected coordinates (H). Open and  
 770 closed symbols represent upper and lower hemispheres. Stars and triangle and associated  
 771 ellipses denote site D197 MT means and local paleomagnetic field direction for mean  
 772 pole of Bangemall Supergroup sills (part of Warakurna LIP) with 95% confidence  
 773 intervals (Wingate et al., 2002), respectively.

774



776

777

**Fig. 9.** Pebble conglomerate tests at Erawandoo Hill sites EHJH5, EHJH6, and EHJH7.

778

(A-D) Two-dimensional projection of the endpoint of the NRM vector during AF and thermal demagnetization in geographic coordinates for clasts EHJH5-2e (A), EHJH5-3m

780

(B), EHJH7-8c.2 (C), and EHJH6-a11c (D). Closed and open symbols represent end

781

points of magnetization projected onto north-east (N-E) and up-east (U-E) planes,

782

respectively. Temperatures for selected thermal demagnetization steps are labeled. (E-G)

783

Equal area stereonet showing directions of magnetization components from clasts

784

(circles) and matrix (squares) from sites EHJH5 (E), EHJH7 (F), and EHJH6 (G). For

785

all clasts, HT components are shown, while for matrix, MT and HT components are

786

shown for EHJH5 and EHJH7, respectively. Open and closed symbols represent upper

787

and lower hemispheres. Stars and associated ellipses denote Fisher HT mean directions

788

and associated 95% confidence ellipse for clasts at site EHJH5 (E) and combined clasts

789

and matrix at sites EHJH7 and EHJH6 (F, G). Triangle and associated ellipse denotes

790

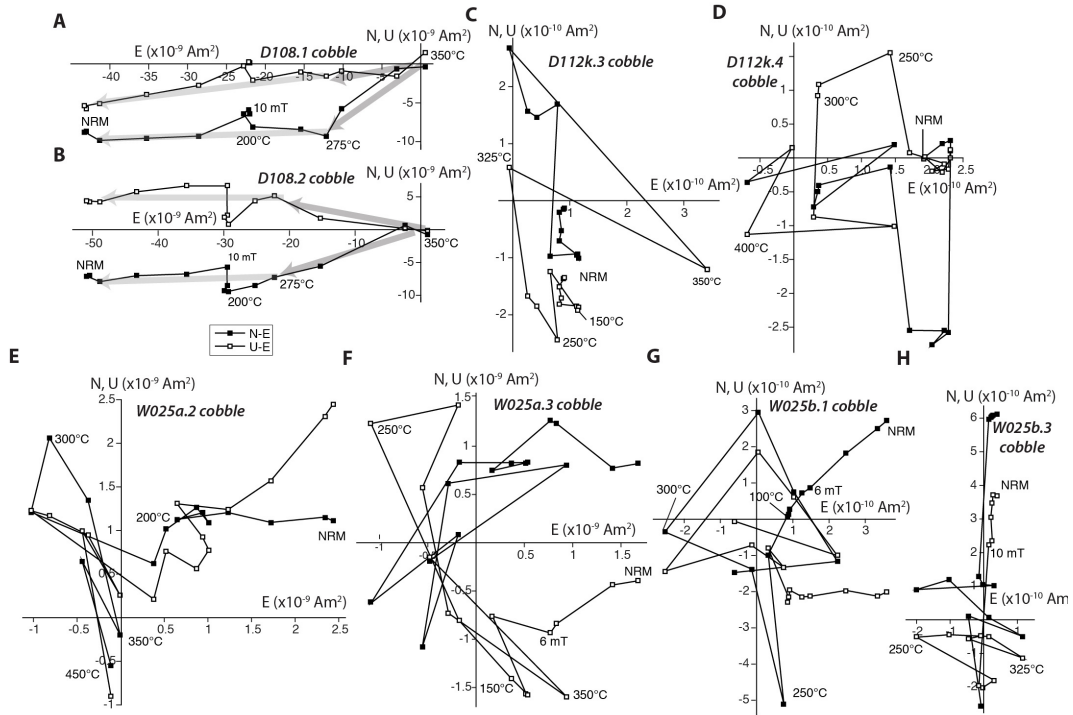
local paleomagnetic field direction and 95% confidence interval for mean pole for

791

Bangemall Supergroup sills (part of Warakurna LIP) (Wingate et al., 2002).

792

793



794

795

796

797

798

799

800

801

802

803

804

805

806

807

808

**Fig. 10.** Paleomagnetism of selected samples from the cobble conglomerate tests. Shown are two-dimensional projections of the endpoint of the NRM vector during AF and thermal demagnetization in geographic coordinates. Open and closed symbols represent end points of magnetization projected onto north-east (N-E) and up-east (U-E) planes, respectively. Peak AC fields and temperatures for selected AF and thermal demagnetization steps are labeled. (A, B) Two subsamples from cobble D108 showing stable demagnetization and homogenous components. (C, D) Two subsamples from cobble D112k showing unstable and inhomogeneous demagnetization behavior. (E, F) Two subsamples from cobble W025a showing unstable and inhomogeneous demagnetization behavior. (G, H) Two subsamples from cobble W025b showing unstable and inhomogeneous demagnetization behavior.



808

809 **References**

- 810 Biggin, A., de Wit, M., Langereis, C., Zegers, T., Voute, S., Dekkers, M., Drost, K.,  
811 2011. Palaeomagnetism of Archaean rocks of the Onverwacht Group, Barberton  
812 Greenstone Belt (southern Africa): Evidence for a stable and potentially reversing  
813 geomagnetic field at ca. 3.5 Ga. *Earth Planet. Sci. Lett.* 302, 314-328.
- 814 Buchan, K.L., 2007. Baked contact test. In: Gubbins, D., Herrero-Bervera, E. (Eds.),  
815 *Encyclopedia of Geomagnetism and Paleomagnetism*, Springer, Dordrecht, The  
816 Netherlands. pp. 35-39.
- 817 Cavosie, A.J., Wilde, S.A., Liu, D., Weiblen, P.W., Valley, J.W., 2004. Internal zoning  
818 and U–Th–Pb chemistry of Jack Hills detrital zircons: a mineral record of early  
819 Archean to Mesoproterozoic (4348–1576 Ma) magmatism. *Precambrian Res.* 135,  
820 251-279.
- 821 Cherniak, D.J., Watson, E.B., 2000. Pb diffusion in zircon. *Chem. Geol.* 172, 5-24.
- 822 Dekkers, M.J., 1989. Magnetic properties of natural goethite-II. TRM behaviour during  
823 thermal and alternating field demagnetization and low-temperature treatment.  
824 *Geophys. J.* 97, 341-355.
- 825 Dunlop, D.J., Özdemir, O., 1997. *Rock magnetism: Fundamentals and frontiers.*  
826 Cambridge University Press, New York. 573 pp.
- 827 Dunn, S.J., Nemchin, A.A., Cawood, P.A., Pidgeon, R.T., 2005. Provenance record of the  
828 Jack Hills metasedimentary belt: Source of the Earth's oldest zircons.  
829 *Precambrian Res.* 138, 235-254.
- 830 Eriksson, K.A., Wilde, S.A., 2010. Palaeoenvironmental analysis of Archaean siliciclastic  
831 sedimentary rocks in the west–central Jack Hills belt, Western Australia with new  
832 constraints on ages and correlations. *J. Geol. Soc. London* 167, 827-840.
- 833 Gomi, H., Ohta, K., Hirose, K., Labrosse, S., Caracas, R., Verstraete, M.J., Hernlund,  
834 J.W., 2013. The high conductivity of iron and thermal evolution of the Earth's  
835 core. *Phys. Earth Planet. Inter.* 224, 88-103.
- 836 Graham, J.W., 1949. The stability and significance of magnetism in sedimentary rocks. *J.*  
837 *Geophysical Research* 54, 131-167.
- 838 Grange, M.L., Wilde, S.A., Nemchin, A.A., Pidgeon, R.T., 2010. Proterozoic events  
839 recorded in quartzite cobbles at Jack Hills, Western Australia: New constraints on  
840 sedimentation and source of >4 Ga zircons. *Earth Planet. Sci. Lett.* 292, 158-169.
- 841 Gubbins, D., Alfè, D., Masters, G., Price, D., Gillan, M., 2004. Gross thermodynamics of  
842 two-component core convection. *Geophys. J. Int.* 157, 1407-1414.
- 843 Hall, A.J., 1986. Pyrite-pyrrhotine redox reactions in nature. *Mineral. Mag.* 50, 223-229.
- 844 Holden, P., Lanc, P., Ireland, T.R., Harrison, T.M., Foster, J.J., Bruce, Z., 2009. Mass-  
845 spectrometric mining of Hadean zircons by automated SHRIMP multi-collector  
846 and single-collector U/Pb zircon age dating: The first 100,000 grains. *Int. J. Mass*  
847 *Spectrom.* 286, 53-63.
- 848 Jaeger, J.C., 1964. Thermal effects of intrusions. *Rev. Geophys.* 2, 443-466.
- 849 Kirschvink, J.L., 1980. The least-squares line and plane and the analysis of  
850 paleomagnetic data: examples from Siberia and Morocco. *Geophys. J. R. Astr.*  
851 *Soc.* 62, 699-718.
- 852 Kirschvink, J.L., Kopp, R.E., Raub, T.D., 2008. Rapid, precise, and high-sensitivity  
853 acquisition of paleomagnetic and rock-magnetic data: Development of a low-

854 noise automatic sample changing system for superconducting rock  
855 magnetometers. *Geochem. Geophys. Geosyst.* 9, Q05Y01,  
856 doi:10.1029/2007GC001856.

857 Lammer, H., Kasting, J.F., Chassefière, E., Johnson, R.E., Kulikov, Y.N., Tian, F., 2008.  
858 Atmospheric escape and evolution of the terrestrial planets and satellites. *Space*  
859 *Sci. Rev.* 139, 399-436.

860 Lowrie, W., 1990. Identification of ferromagnetic minerals in a rock by coercivity and  
861 unblocking temperature properties. *Geophys. Res. Lett.* 17, 159-162.

862 Maas, R., Kinny, P.D., Williams, I.S., Froude, D.O., Compston, W., 1992. The Earth's  
863 oldest known crust: A geochronological and geochemical study of 3900-4200 Ma  
864 old detrital zircons from Mt. Narryer and Jack Hills, Western-Australia. *Geochim.*  
865 *Cosmochim. Acta* 56, 1281-1300.

866 McElhinny, M.W., 1964. Statistical significance of the fold test in paleomagnetism.  
867 *Geophys. J. R. Astron. Soc.* 8, 338-340.

868 Mezger, K., Krogstad, E.J., 1997. Interpretation of discordant U-Pb zircon ages: An  
869 evaluation. *J. Metamorphic Geol.* 15, 127-140.

870 Nimmo, F., Price, G.D., Brodholt, J., Gubbins, D., 2004. The influence of potassium on  
871 core and geodynamo evolution. *Geophys. J. Int.* 156, 363-376.

872 Özdemir, Ö., Dunlop, D.J., 1996. Thermoremanence and Néel temperature of goethite.  
873 *Geophys. Res. Lett.* 23, 921-924.

874 Pidgeon, R.T., Wilde, S.A., 1998. The interpretation of complex zircon U-Pb systems in  
875 Archaean granitoids and gneisses from the Jack Hills, Narryer Gneiss Terrane,  
876 Western Australia. *Precambrian Res.* 91, 309-322.

877 Pirajno, F., 2004. Metallogeny in the Capricorn Orogen, Western Australia, the result of  
878 multiple ore-forming processes. *Precambrian Res.* 128, 411-439.

879 Rasmussen, B., Fletcher, I.R., Muhling, J.R., Wilde, S.A., 2010. In situ U-Th-Pb  
880 geochronology of monazite and xenotime from the Jack Hills belt: Implications  
881 for the age of deposition and metamorphism of Hadean zircons. *Precambrian Res.*  
882 180, 26-46.

883 Schmidt, P.W., 2014. A review of Precambrian palaeomagnetism of Australia:  
884 Palaeogeography, supercontinents, glaciations and true polar wander. *Gondwana*  
885 *Res.* 25, 1164-1185.

886 Smirnov, A.V., Evans, D.A.D., Ernst, R.E., Söderlund, U., Li, Z.-X., 2013. Trading  
887 partners: Tectonic ancestry of southern Africa and western Australia, in Archaean  
888 supercratons Vaalbara and Zimgarn. *Precambrian Res.* 224, 11-22.

889 Spaggiari, C.V., 2007a. The Jack Hills greenstone belt, Western Australia Part 1:  
890 Structural and tectonic evolution over >1.5 Ga. *Precambrian Res.* 155, 204-228.

891 Spaggiari, C.V., Pidgeon, R.T., Wilde, S.A., 2007. The Jack Hills greenstone belt,  
892 Western Australia Part 2: Lithological relationships and implications for the  
893 deposition of  $\geq 4.0$  Ga detrital zircons. *Precambrian Res.* 155, 261-286.

894 Spaggiari, C.V., Wartho, J.-A., Wilde, S.A., 2008. Proterozoic deformation in the  
895 northwest of the Archaean Yilgarn Craton, Western Australia. *Precambrian Res.*  
896 162, 354-384.

897 Swanson-Hysell, N.L., Feinberg, J.M., Berquó, T.S., Maloof, A.C., 2011. Self-reversed  
898 magnetization held by martite in basalt flows from the 1.1-billion-year-old  
899 Keweenawan rift, Canada. *Earth Planet. Sci. Lett.* 305, 171-184.

- 900 Swanson-Hysell, N.L., Maloof, A.C., Kirschvink, J.L., Evans, D.A.D., Halversong, G.P.,  
901 Hurtgen, M.T., 2012. Constraints on Neoproterozoic paleogeography and  
902 paleozoic orogenesis from paleomagnetic records of the Bitter Springs Formation,  
903 Amadeus Basin, Central Australia. *Am. J. Sci.* 312, 817-884.
- 904 Tarduno, J.A., Cottrell, R.D., Watkeys, M., Hofmann, A., Doubrovine, P.V., Mamajek,  
905 E.E., Liu, D., Sibeck, D.G., Neukirch, L.P., Usui, Y., 2010. Geodynamo, solar  
906 wind, and magnetopause 3.4 to 3.45 billion years ago. *Science* 327, 1238-1240.
- 907 Tarduno, J.A., Cottrell, R.D., 2013. Signals from the ancient geodynamo: A  
908 paleomagnetic field test on the Jack Hills metaconglomerate. *Earth Planet. Sci.*  
909 *Lett.* 367, 123-132.
- 910 Tarduno, J.A., Blackman, E.G., Mamajek, E.E., 2014. Detecting the oldest geodynamo  
911 and attendant shielding from the solar wind: Implications for habitability. *Phys.*  
912 *Earth Planet. Inter.* 233, 68-87.
- 913 Torsvik, T.H., Van der Voo, R., Preeden, U., Mac Niocaill, C., Steinberger, B.,  
914 Doubrovine, P.V., van Hinsbergen, D.J.J., Domeier, M., Gaina, C., Tohver, E.,  
915 Meert, J.G., McCausland, P.J.A., Cocks, L.R.M., 2012. Phanerozoic polar  
916 wander, palaeogeography and dynamics. *Earth Sci. Rev.* 114, 325-368.
- 917 Veikkolainen, T., Pesonen, L.J., Evans, D.A.D., 2014. PALEOMAGIA: A PHP/MYSQL  
918 database of the Precambrian paleomagnetic data. *Stud. Geophys. Geod.* 58, 425-  
919 441.
- 920 Watson, G.S., 1956. A test for randomness. *Mon. Not. R. Astr. Soc.* 7, 160-161.
- 921 Wilde, S.A., Pidgeon, R.T., 1990. Geology of the Jack Hills metasedimentary rocks. In:  
922 Ho, S.E., Glover, J.E., Myers, J.S., Muhling, J.R. (Eds.), Third International  
923 Archaean Symposium (Perth) Excursion Guidebook 21, University of Western  
924 Australia Extension Publication, Perth. pp. 82-95.
- 925 Wilde, S.A., 2010. Proterozoic volcanism in the Jack Hills Belt, Western Australia: Some  
926 implications and consequences for the World's oldest zircon population.  
927 *Precambrian Res.* 183, 9-24.
- 928 Wingate, M.T.D., Pisarevsky, S.A., Evans, D.A.D., 2002. Rodinia connections between  
929 Australia and Laurentia: no SWEAT, no AUSWUS? *Terra Nova* 14, 121-128.
- 930 Wingate, M.T.D., Pirajno, F., Morris, P.A., 2004. Warakurna large igneous province: A  
931 new Mesoproterozoic large igneous province in west-central Australia. *Geology*  
932 32, 105-108.
- 933 Ziegler, L.B., Stegman, D.R., 2013. Implications of a long-lived basal magma ocean in  
934 generating Earth's ancient magnetic field. *Geochem. Geophys. Geosyst.* 14, doi:  
935 10.1002/2013GC005001.

936